Long-term non-invasive interrogation of human dorsal root ganglion neuronal cultures on an integrated microfluidic multielectrode array platform†

H. A. Enright,[a] S. H. Felix,[b] N. O. Fischer,[a] E. V. Mukerjee,[b] D. Soscia,[b] M. Mcnerney,[a] K. Kulp,[a] J. Zhang,[c] G. Page,[c] P. Miller,[c] A. Ghetti,[c] E. K. Wheeler*[b] and S. Pannu[b]

Scientific studies in drug development and toxicology rely heavily on animal models, which often inaccurately predict the true response for human exposure. This may lead to unanticipated adverse effects or misidentified risks that result in, for example, drug candidate elimination. The utilization of human cells and tissues for *in vitro* physiological platforms has become a growing area of interest to bridge this gap and to more accurately predict human responses to drugs and toxins. The effects of new drugs and toxins on the peripheral nervous system are often investigated with neurons isolated from dorsal root ganglia (DRG), typically with one-time measurement techniques such as patch clamping. Here, we report the use of our multi-electrode array (MEA) platform for long-term noninvasive assessment of human DRG cell health and function. In this study, we acquired simultaneous optical and electrophysiological measurements from primary human DRG neurons upon chemical stimulation repeatedly through day *in vitro* (DIV) 23. Distinct chemical signatures were noted for the cellular responses evoked by each chemical stimulus. Additionally, the cell viability and function of the human DRG neurons were consistent through DIV 23. To the best of our knowledge, this is the first report on long-term measurements of the cell health and function of human DRG neurons on a MEA platform. Future generations will include higher electrode numbers in customized arrangements as well as integration with different tissue types on a single device. This platform will provide a valuable testing tool for both rodent and human cells, enabling a more comprehensive risk assessment for drug candidates and toxicants.

Introduction

The development of new drug entities and the study of potential toxicants almost always involve the use of animal models, which are complicated by relevance as well as ethical issues. Frequently, the animal models available and chosen for the pre-clinical testing of drugs do not accurately predict their clinical safety, efficacy and off-target effects in humans.[1,2] Therefore, new human-tissue based methods are being developed to (1) circumvent the risks inherent in cross-species extrapolation and (2) enable testing of potential new drug entities on human tissues earlier in the drug development pipeline.

One approach for facilitating the assessment of therapeutics prior to human use and the evaluation of the risk of potential toxins to which humans are exposed is to develop chip-based platforms that support human organ-specific cells and tissues.[3,4] By enabling measurements of viability and function after compound exposure, these technologies can provide mechanistic information about the proposed therapeutic compounds and provide valuable insight into their potential safety, efficacy, pharmacokinetics and pharmacodynamics concerns prior to testing the chemical in higher organisms.

An important aspect of testing new drugs and other substances for toxicity is to understand their effects on the peripheral nervous system, which is frequently modeled by neurons that have been dissociated from dorsal root ganglia (DRG). DRG, located along the spinal nerves, house the cell bodies of sensory neurons whose dendrites are located in the skin, muscles, tendons, joints and internal organs. These neurons have a variety of sensory receptors that are activated by mechanical, thermal, chemical, and noxious stimuli,

[a]*Biosciences and Biotechnology Division, Lawrence Livermore National Laboratory, Livermore, CA, USA*
[b]*Engineering, Lawrence Livermore National Laboratory, Livermore, CA, USA.*
E-mail: Wheeler16@llnl.gov
[c]*Anabios, Inc., San Diego, CA, USA*
†Electronic supplementary information (ESI) available. See DOI: 10.1039/c5an01728a

making them the model system of choice for studying the transmission of painful stimuli.[5]

Lack of access to primary human sensory neurons has hindered the understanding of the physiology of pain in humans;[6] most investigations have been performed on neurons retrieved from ganglionectomized chronic pain patients or fetal and autopsy tissues. Studies of intact tissues are limited; these studies typically characterize the expression of nociceptors and document the changes that occur to these receptors in terms of number and localization after injury.[7–12]

In a few cases, viable human tissues have been dissociated into single neurons and utilized to characterize receptor function using traditional electrophysiological methods, such as patch clamping, to monitor alterations in the electrophysiological response.[13–26] Studies of dissociated human dorsal root ganglion (hDRG) neurons have described changes in electrophysiology and ion channel function due to changing culture conditions,[23] exposure to viral proteins,[25] drugs, and chemicals.[24,26–29] While these techniques are very informative, they are restricted to individually interrogating single cells. In addition, these interrogations are typically limited to endpoint analyses, precluding kinetic or extended measurements on a single cell or population. As such, collecting large, statistically-relevant data sets is time-consuming and labor-intensive.

Microelectrode arrays (MEAs) have the advantage of being able to non-invasively and repeatedly record extracellular electrical signals from cell populations for long periods (days to months) without causing damage to the cell membrane.[30,31] MEAs record the extracellular potentials generated by the spike activity of single or multiple neurons that may be on or near a particular electrode. To date, MEAs have been employed to interrogate neural activity in cultures of animal cells and, in some cases, cultures derived from human stem cells.[32–35]

In this study, we have developed a platform incorporating a MEA to investigate the response of viable, dissociated hDRG neurons, providing data about the behavior of the neurons in a controlled, physiological environment. The platform was designed to enable: tightly regulated conditions in the cell growth chamber to maintain cell health; non-invasive electrophysiology recordings using a sixteen electrode microelectrode array; compatibility with brightfield and fluorescent microscopy to monitor cell viability and responses to chemical exposures; and automated fluid exchange for chemical exposures using microfluidics. The surfaces of the platform have been designed to support cell growth and adherence and have demonstrated long-term biocompatibility.

Our engineered platform and culturing conditions have been optimized to support dissociated adult hDRGs derived from human organ donors. Primary human tissues and cell cultures provide reliable human-relevant data by retaining the phenotype and functionality of normal *in vivo* tissue. The use of adult tissues helps ensure that the neurons are fully developed with all of the necessary pathways and receptors present.[26] Although many of the electrophysiological and pharmacological features of DRG neurons appear to be conserved across species, several studies have highlighted key differences between the traditional rat model and human DRG neurons. For example, the array of ion channels expressed in human DRG neurons is not identical to rat DRG neurons and the effects of targeted knock-outs or mutations are therefore different.[36,37]

In this study, which is the first to incorporate hDRGs into a platform with an integrated MEA, we assessed neuronal health and function and validated our platform by exposing cells to various chemicals known to elicit neuronal response. These chemicals include (1) capsaicin, a toxin that models neural pain responses by stimulating specific neuronal receptors (transient receptor potential cation channel subfamily V member 1, TRPV1), (2) ATP, an activator of two types of neural and glia receptors (P2X, P2Y), and (3) KCl, which causes membrane depolarization in neurons.

Experimental

Materials

Poly-D-lysine, adenosine triphosphate disodium salt hydrate, calcium chloride, magnesium chloride, HEPES, glucose, penicillin–streptomycin, pluronic acid F-127 and capsaicin were purchased from Sigma Aldrich (St Louis, MO). Sodium chloride was purchased from Fisher Scientific (Waltham, MA). Laminin and DMEM-F12 were purchased from Invitrogen (Carlsbad, CA). Horse serum and Hank's Balanced Salt Solution (HBSS, $+Ca^{2+}$, $+Mg^{2+}$) were purchased from Life Technologies (Carlsbad, CA). Human nerve growth factor (hNGF) and human glial-derived neurotrophic factor (hGDNF) were purchased from Neuromics (Edina, MN). Gem21 was purchased from Gemini Bioproducts (West Sacramento, CA). KCl was purchased from Sigma Aldrich (St Louis, MO). Fluo-8 was purchased from AAT Bioquest (Sunnyvale, CA). AZ4620 photoresist, as well as AZ and AZ400K developers were purchased from AZ Electronic Materials (Somerville, NJ). H20E conductive silver epoxy and 301-2 potting epoxy were purchased from Epoxy Technology (Billerica, MA).

Multielectrode array (MEA)

The microelectrode array consisted of sixteen electrodes of 20 μm diameter. The top two rows and the bottom two rows had a pitch of 200 μm. The middle two rows are separated by a distance of 220 μm. The fabrication of the multielectrode array (MEA) is shown in Fig. 1. Four inch SiO_2 wafers were sputter-coated with a 200 Å titanium adhesion layer and a 2500 Å platinum trace layer. The metal trace and electrode patterns were defined using photolithography and a plasma enhanced chorine metal etch (ULVAC). The photoresist was removed using an O_2 plasma etch and the wafers were pre-treated with a VM652 adhesion promoter prior to applying a 2 μm spin coated polyimide film. The polyimide was soft baked at 95 °C for 10 min and subsequently cured in an oven at 375 °C. Next, a sputtered aluminum etch mask was deposited, photolithographically patterned, and wet etched (PAN – phosphoric,
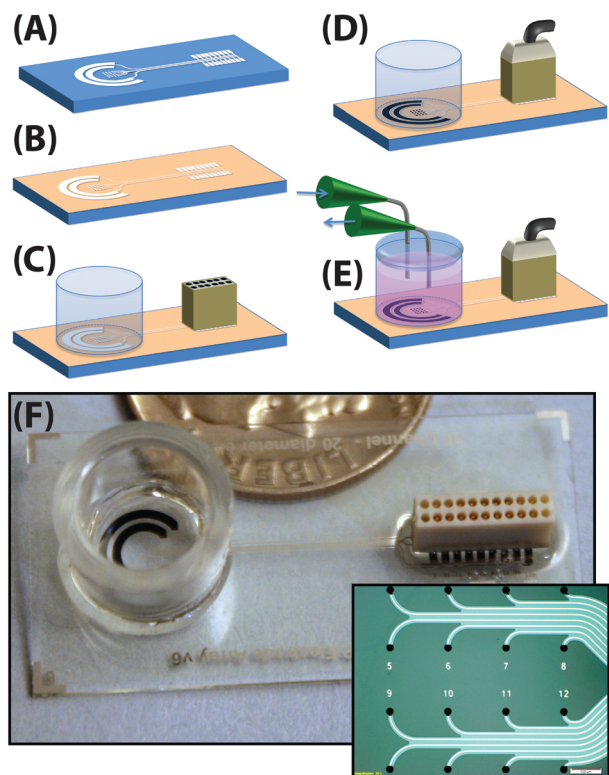
Fig. 1 Process flow for device fabrication and assembly. (A) Metal electrodes and traces are patterned on glass. (B) Polyimide is used as a passivation layer for the traces. (C) A polystyrene well and an electronic connector are attached. (D) The MEA is electroplated with platinum black to increase the electrode surface area and reduce impedance. (E) Prior to testing, microfluidics are connected in order to introduce challenge compounds for electrophysiological recordings. (F) A completed device after electroplating (inset: brightfield micrograph of electroplated MEA).

acetic and nitric acid). The polyimide was then anisotropically dry etched using O_2 plasma to expose the electrodes and contact pads. The aluminum etch mask was removed with PAN. Using a dicing saw, the individual MEA devices were separated and FlipChip bonded to Omnetics 18-channel connectors utilizing conductive epoxy. The connectors were then potted in epoxy to maintain mechanical integrity. Polystyrene rings were glued to the devices around the MEA region using silicone adhesive to define the cell-culture wells.

Platinum was electroplated onto the exposed electrode surfaces to decrease impedance and enhance the signal-to-noise ratio of electrophysiological recordings. Platinum black was electroplated on the electrodes in a solution of 0.1 M nitric acid with 192 mg l^{-1} sodium hexachloroplatinate IV hexahydrate, using a three-electrode cell consisting of a Pt counter electrode, an Ag/AgCl reference electrode, and the surface electrode as the working electrode. One hundred staircase cyclic voltammetry (CV) cycles were performed with a potential range of −100 mV to +100 mV at a scan rate of 25 mV s^{-1}. To verify the electrode function, electrochemical characterization of the electrodes was performed after electroplating.

Cyclic voltammetry (CV) and electrochemical impedance measurements were made with a Princeton Applied Research (PAR) potentiostat using vendor-supplied software. All measurements were made on a three-electrode cell using a Pt counter electrode, an Ag/AgCl reference electrode, and phosphate-buffered saline (pH 7.4) as the electrolyte. Potential cycling for the CVs was performed between −600 mV and +600 mV at a scan rate of 100 mV s^{-1}. Electrochemical impedance spectroscopy (EIS) data were measured from 100 Hz to 10 MHz using a 10 mV rms sine wave. A final measurement of electrode impedance was obtained from the AlphaLab SnR (Alpha Omega, Alpharetta, GA) at 1000 kHz immediately prior to the experiment.

Cell seeding

Primary human dorsal root ganglion (hDRG) neurons were obtained from Anabios, Inc. Human DRG cell cultures were established as previously described.[26] All human DRG samples were obtained by Anabios from an ethically consented organ donor in the USA. The donor in this study was a 31 year old Caucasian female, with a body mass index of 25.9; the cause of death was a head trauma. After isolation, cells were seeded onto poly-D-lysine/laminin coated MEAs and incubated at 37 °C and 5% CO_2. Three devices were seeded, with approximately 300–600 neurons placed in each well. Cells were maintained by replacing half of the growth media (DMEM F-12 supplemented with 10% horse serum, 25 ng mL^{-1} of hNGF, 25 ng mL^{-1} hGDNF, Gem21 and penicillin–streptomycin) every three days. No antimitotics were added to the cultures. Cells were characterized by immunocytochemistry assays and the response to chemical stimuli was measured optically and with electrophysiology.

Immunocytochemistry

Cells were fixed with 4% paraformaldehyde, rinsed three times with phosphate buffered saline (PBS) and permeabilized with cold 100% methanol. Cells were blocked with 10% goat serum for 45 minutes at room temperature and stained with primary antibodies overnight at 4 °C. Primary antibodies included a mouse antibody to neuron-specific class III beta-tubulin (tuj-1, Neuromics, Edina, MN, diluted at 1 : 100) and a rabbit antibody to vanilloid receptor (TRPV1) (Pierce, Rockford, IL, diluted at 1 : 300). The next day, cells were washed three times with 1× PBS, stained with secondary antibodies for 1 hour at 37 °C and washed three times with 1× PBS before imaging. Secondary antibodies included a goat antibody to mouse AlexaFluor 488 (diluted at 1 : 100) and a goat antibody to rabbit AlexaFluor 594 (diluted at 1 : 100) (Life Technologies, Eugene, OR).

Chemical challenge using a fluidic system

Prior to the chemical challenge experiments, MEAs were removed from the incubator and the maintenance cap on our MEA platform was replaced with a custom made fluidic cap as illustrated in Fig. 1e. The ports on the cap were attached to the inlet and outlet lines of a fluidic handling system (FloPro). The

MEA platform was then placed in a custom-made heated stage that permitted the connection of the electrodes to the recording system while maintaining a constant temperature. The temperature of the cultures was monitored using a thermocouple and a controller (Omega, Stamford, CT). Next, chemical challenges and buffer rinses were delivered to the cells using the FloPro system with a controlled flow rate of 1.5 mL min^{-1}.

The dilution and rinse buffer consisted of 145 mM NaCl, 3 mM KCl, 2 mM CaCl$_2$, 1 mM MgCl$_2$, 10 mM HEPES and 10 mM glucose. 500 nM capsaicin, 10 mM ATP and 30 mM KCl were used for hDRG challenges and were prepared in the buffer. For 30 mM KCl, the concentration of NaCl in the dilution buffer was adjusted to 120 mM. The osmolarity of the challenge solutions and the buffer was between 290 and 310 mOsm and the pH was between 7.2 and 7.4. Cells were challenged in the following order: ATP, capsaicin and KCl, with each challenge followed by a buffer rinse and a ten-minute wait time before the next challenge solution. Cells were repeatedly challenged over DIV 23, with testing on DIV 15, 16, 19 and 23.

Calcium imaging

Prior to chemical challenging, cells were incubated with 4–5 μM of Fluo-8 AM calcium indicator (λ_{ex} = 490 nm, λ_{em} = 525 nm) in HBSS buffer containing 20 mM HEPES and 0.02% pluronic acid for 20–30 minutes at 37 °C and then rinsed with HBSS/HEPES buffer (osmolarity = 290–310 mOsm, pH = 7.2–7.4). A Leica inverted microscope controlled using Metamorph imaging software (Molecular Devices, Sunnyvale, CA) was used for imaging. During each chemical challenge, images were acquired every 500–600 ms using a GFP filter set. A baseline of approximately 10 seconds was acquired before chemical exposure. Calcium data were analyzed by selecting regions of interest (ROI) in ImageJ over each neuron in the field of view. Background intensity was subtracted from the average pixel intensities for each ROI and the change in intensity from the average of the baseline ($\Delta F/F_0$) was calculated for neurons over time. Neurons with $\Delta F/F_0$ that were more than three times the standard deviation of the baseline were considered responsive.

Electrophysiological recording and analysis

Voltage recordings from the MEA were collected using a multi-channel recording system (AlphaLab SnR, Alpha Omega, Alpharetta, GA) and were sampled at a frequency of 22.3 kHz and bandpass filtered between 268 and 8036 Hz.

Single unit spikes were detected from the continuously recorded extracellular voltage signal offline. A custom MATLAB script was used to improve detection of spikes with a low signal-to-noise ratio, compared to conventional amplitude threshold detection. In recent years, researchers have begun to employ enhanced spike detection algorithms, particularly in applications involving microelectrode arrays implanted *in vivo*.[38–43] Due to the high value of the human cell cultures described in this paper, such an approach was taken to extract as much neural spike information as possible. Some spike detection methods, such as those involving template matching and Bayesian approaches, rely on large sets of data to train the algorithm, and can be computationally demanding.[39,41] In contrast, other methods use a relatively small window of data to detect spikes by making some assumptions about the noise and signal characteristics. These include transformations such as the nonlinear energy operator[44] or likelihood based criteria.[43] The MATLAB script used in this analysis employs such a scheme in the form of a weighted sum of squared residuals (WSSR) statistic, a chi-squared based test used in event and fault detection applications.[45–48] The operator is given as follows:

$$M(k) = \frac{1}{\sigma} \sum_{j=0}^{N} V(k+j)^2$$

where $V(k)$ is the recorded voltage at sample k, with variance σ, and N is the size of the sliding window over which the WSSR is evaluated. In the absence of a neural signal, it is assumed that $V(k)$ is zero mean and white (uncorrelated). Refer to Mehra and Peschon[45] and Willsky and Jones[46] for a derivation of this metric. The formulation is equivalent to that of a chi-squared test metric with the sample size being the chosen window length, N. As such, a pattern in the signal resulting from a neural spike will be significantly amplified in this metric relative to the background noise. A window length of N = 100 samples was used, and a spike was determined to be present when $M(k)$ deviated from its mean more than 10 times the standard deviation of $M(k)$ in the presence of no spikes.

After detecting spikes, spike waveforms spanning 6.7 ms were saved along with time stamps associated with each waveform. The time stamp of the event was determined from the peak in $M(k)$ near the crossing of the threshold. A refractory period of 3.4 ms was imposed to prevent detection of the same waveform multiple times. Spikes were also screened to remove noise artifacts that occurred simultaneously on all the channels. It is possible, in extracellular electrophysiological recordings, that a single electrode may record spikes from multiple neurons. However, the waveforms that result from the action potentials of a single neuron will be characteristic, and a classification scheme can be employed to sort spikes by their source neuron.[49] Since this only occurred in a few instances, spike waveforms were sorted by inspection rather than using an automated algorithm.

Statistics

Data were compiled in Microsoft Excel and analyzed using Prism 6 (GraphPad, La Jolla, CA). Statistical significance between multiple groups was assessed using one-way ANOVA. Pairwise comparisons were analyzed using a Tukey's multiple comparisons test. Where appropriate, data are expressed as the mean ± standard deviation.

Results and discussion

To demonstrate the ability of the engineered platform to support the long-term maintenance of healthy adult neurons and allow for the measurement of repeated responses to chemical challenges, we cultured dissociated DRG neurons from a human donor on three MEA-containing devices. The design and assembly of the platform are shown in Fig. 1. The impedances for functional electrodes on the MEA platforms at 1 kHz were 126 ± 69 kΩ ($n = 38$) for our 20 μm electrodes. Electrodes on the MEA platform were considered non-functional if the impedance exceeded 1 MΩ. Collectively, the three devices used in these studies had a 94% yield for functional electrodes. The background noise on electrodes with neural activity was 5.3 μV root-mean-square (RMS) or less. The performance of the device compared favorably to other custom and commercially available MEAs.[34,50,51] Other MEA systems have electrode sizes ranging from 10 to 100 μm and a center to center space from 50 to 400 μm. Impedance depends on both electrode size and electrode material and is typically in the range of 100 kΩ to several MΩ at 1 kHz; lower impedance within this range results in less noise when measuring single unit recordings. Studies using MEAs have reported background noise levels of 10–20 μV in amplitude or approximately 7–14 μV RMS. While sixteen channels is a relatively low number (compared to 60 or more channels in most other MEA systems), this channel count was chosen to balance area covered and cell visibility in optical imaging. Future generations of this platform will be designed to accommodate different types of tissue and multi-modal sensing. To this end, they will have not only more channels, but also custom geometric arrangements and electrode coatings that are not commercially available.

Brightfield images of a representative population of neurons and their supporting glia, isolated from the donor dorsal root ganglia and seeded onto our MEA platform, are shown in Fig. 2. Both single neurons and small clusters of neurons were observed within the cultures. Neuronal cell clustering within primary cultures is common and is often a result of the dissociation process.[52,53] Cells were located on top of electrodes as well as in the insulating field. Previous studies have shown that while close coupling of cells to electrodes can increase the amplitude of an extracellularly recorded signal, it is possible to detect action potentials from neurons up to ~100 μm from electrodes.[54,55] Heterogeneity in size within cultures for DRG neurons is also common; soma size for human DRG neurons is reported to range from <28 μm to 58 μm.[24,26]

The neuronal cultures seeded on the MEA platform were successfully maintained through DIV 23 as evidenced by the robust repeated responses to chemical stimuli, measured both optically and with electrophysiology. Fig. 2(A)–(C) show the same region of the MEA on DIV 15, 19 and 23. Although the neurons and supporting glial mat have shifted over the course of the experiment, the cells continued to respond to chemical stimulation. The long-term culture of the hDRG cells on our MEA platform compares well with other neuronal cultures in the literature. Human derived neurons (pluripotent stem cells) have been interrogated on other MEAs up to a month in culture.[56,57] Primary rodent neuronal cultures have been maintained much longer with reports ranging from one month[58,59]
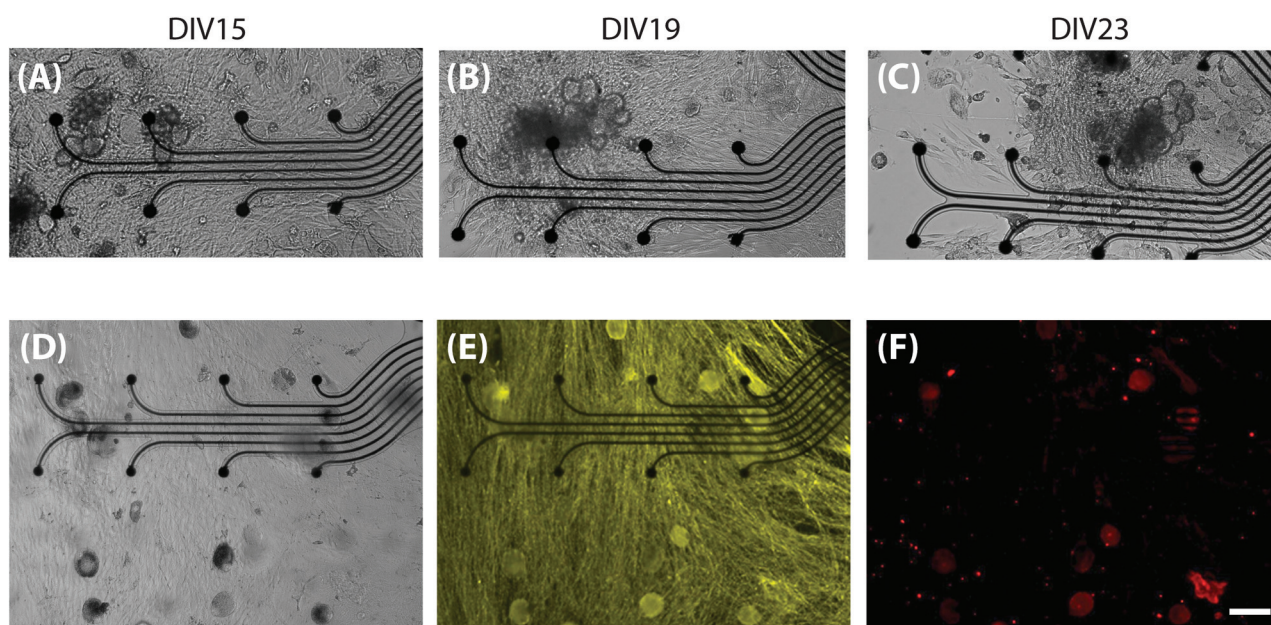

Fig. 2 Long-term culture and immunocytochemistry of hDRG neurons on MEA. (A–C) Representative brightfield images of hDRG neurons and glia on a single device through DIV23. (D) Brightfield image of hDRG neurons. (E) Tuj-1 outgrowth stain for neurons and neuronal processes. (F) Neuronal capsaicin receptor (TRPV-1) staining. Scale bar = 100 μm.

to fifteen months *in vitro*.[30] While human derived cells have been tested long-term on MEAs, our MEA platform is the first to demonstrate the long-term culture of primary human DRG neurons. To characterize the receptor composition of the neuronal population, devices were chemically fixed at the end of the experimental time frame and cells were immunostained for neuron-specific markers. Fig. 2D is the corresponding brightfield image for tuj-1 staining of neuron specific class III β-tubulin (Fig. 2E) and capsaicin-specific vanilloid receptors (TRPV1) (Fig. 2F). The tuj-1 antibody binds specifically to neurons and axons; this antibody was used to visualize the dense network of neuronal processes for our cultures across the entire MEA platform (Fig. 2E). We also stained for neuronal capsaicin receptors within the same culture (Fig. 2F) to verify that our cultures can be activated by chemical stimulation with capsaicin. TRPV1 is highly expressed in polymodal nociceptors and is canonically activated by capsaicin, an ingredient in chili peppers, as well as high heat and low pH. Activation of the receptor causes depolarization of the neuron membrane by opening a calcium permeable non-selective cation channel. Fig. 2F shows that some of the neurons within our culture are positive for TRPV1. Note that not all of the neurons are uniformly fluorescent. This is consistent with a heterogeneous DRG culture containing neurons with varying degrees of TRPV1 receptor expression.

To validate neuronal health and responsiveness to chemicals known to elicit cellular response, changes in calcium dynamics and evoked action potentials were simultaneously monitored after sequential addition of ATP, capsaicin and KCl ($n = 3$). Chemical stimulation that produces a change in membrane polarization promotes an increase in intracellular calcium, so that calcium response can be used as an indicator of neuron excitability.[25] In addition, increased intracellular calcium levels, either *via* mobilization of calcium stores or through calcium influx through calcium channels, are an early indication of neurotoxicity. The ability of our platform to simultaneously monitor calcium dynamics and electrophysiology is a distinct advantage for understanding the effects of compound exposure.

Changes in the intracellular calcium concentration were measured by visualizing the flux of a calcium-specific fluorescent dye and are shown in Fig. 3. Typical intracellular calcium levels for hDRG neurons and supporting glia are shown for cultures before (Fig. 3A) and after exposure to 10 mM ATP (Fig. 3B). Upon stimulation with ATP, a significant influx of calcium occurred in both neurons and their surrounding glia (3B), although a signal from the glia occurred *ca.* 2 s after a peak neuron signal (data not shown). A single representative calcium response for a neuron exposed to each of the three chemical challenges is shown in Fig. 3C ($n = 1$).

Exposure to the chemicals induced a rapid influx of calcium into the cell, followed by a gradual decrease to baseline over time. The measurement time shown represents the addition of the chemical and does not include the time of buffer rinse or chemical washout. Acharjee *et al.* showed a
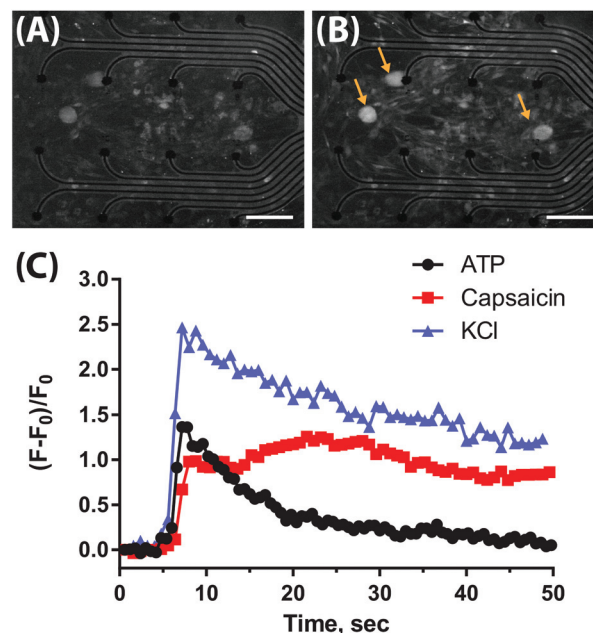

Fig. 3 Optical imaging of calcium dynamics in stimulated hDRG neurons. (A) hDRG cells before ATP exposure. (B) Peak optical response for both neurons (orange arrows) and glia after ATP. (C) Representative optical responses for a neuron on our MEA upon ATP, capsaicin and KCl stimulation. Scale bar = 100 μm.

similar rapid response of human fetal DRG neurons to 35 mM KCl.[25] Exposing the cultures to 500 nM capsaicin also caused a rapid change in intracellular calcium levels; these results are consistent with reports by Anand *et al.* of calcium response to capsaicin in adult human DRG neurons.[15–17]

Concurrent with the optical imaging, the electrophysiological responses of the neurons were measured after stimulation with ATP, capsaicin and KCl. In the peripheral nervous system, generation of action potentials occurs through stimulation of neuronal receptors. An action potential is an event that occurs once a cell's transmembrane potential reaches a certain threshold (−55 mV). Upon stimulation, rapid Na^+ influx causes depolarization of the cell (rise in peak). Repolarization (fall of peak) of the cell occurs through closure of Na^+ channels and opening of K^+ channels, which initiates an efflux of K^+ ions. This efflux eventually leads to the cell returning to its resting membrane potential.[60] Spike events measured extracellularly resemble the shape of an action potential, but are somewhat distorted since they are not directly measuring the potential across the cell membrane. The amplitude of extracellular recordings is typically 20 to 500 μV depending on cell size, electrode location, impedance, and other factors.[34,50,51] Representative extracellular responses recorded from an electrode upon ATP exposure are shown in Fig. 4, with a portion of a spike train shown in Fig. 4A. An expanded view representing spike amplitude and shape is shown for three action potentials in Fig. 4B, and an overlay of individual spike waveforms for recorded spikes is shown in Fig. 4C.
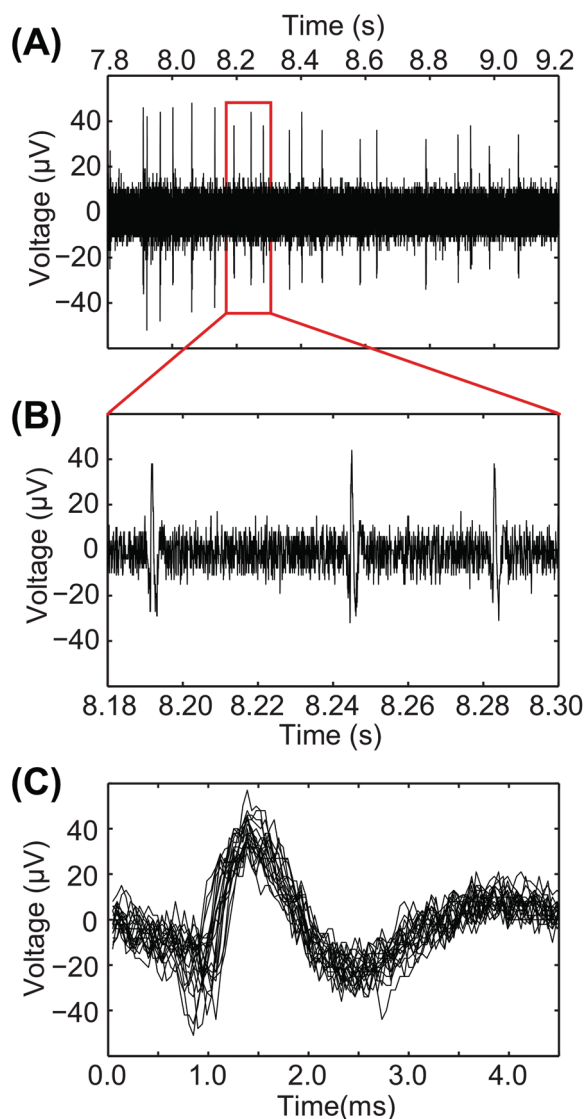
(A)

(B)

(C)

Fig. 4 Extracellular recording of hDRG neuron response to ATP at DIV23. (A) Representative spike train from a single neuron after challenge. (B) Detailed image of spikes from (A). (C) Superimposed spikes from the neuron demonstrating consistency of waveform.

Within our recordings, we captured spikes with a signal to noise ratio (SNR) as low as 14 dB, which is defined as

$$\text{SNR} = \left(\frac{\text{peak to peak amplitude of spike waveform}}{\text{RMS of background noise}}\right)^2$$

Even though these spike trains were visible, a simple threshold applied to the instantaneous voltage amplitude would either overlook these spikes or overpopulate the data set with excessive false positives, making subsequent spike sorting unreliable. For example, a commonly used spike detection criterion is a threshold on the voltage amplitude that equals 4 to 5 times the standard deviation of the background noise.[38,39,61] This equates to detecting spikes with a minimum SNR of 64 as defined above. The enhanced spike detection
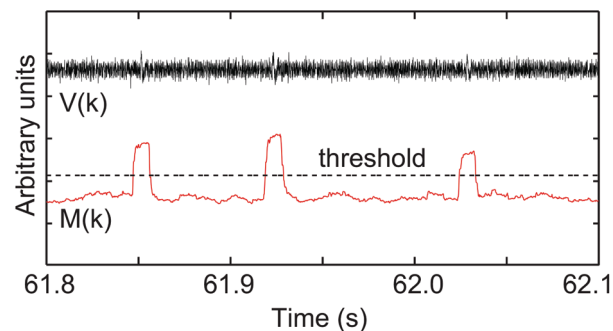

Fig. 5 Example of the original electrophysiological signal and the WSSR statistic. Top: the voltage signal measured from the MEA exhibits three spikes with low signal to noise ratios. Bottom: the WSSR statistic, $M(k)$, results in larger peaks around the spikes that are more easily detected with a threshold.

algorithm described in the Methods section was used on all data sets. Fig. 5 illustrates the comparison between a voltage trace recorded from the MEA and the enhanced metric, $M(k)$. The resulting peaks were easily detected with a simple threshold after enhancement.

Time stamps from the spikes detected after enhancement were organized into raster plots to illustrate the overall activity upon stimulation of the hDRG cultures with ATP (Fig. 6A), KCl (Fig. 6B) and capsaicin (Fig. 6C). Raster plots are commonly used to visualize neural activity by representing each occurrence of a spike by a tick mark along a time axis.[34] These raster plots include the repeated challenges on the three devices over several different days *in vitro*. The responses obtained for each chemical stimulus were similar across the various DIV test days, demonstrating that the device maintained cellular health for longer than 3 weeks. We observed no significant differences ($p > 0.05$) in chemically evoked responses in terms of spike number and median interspike interval (ISI) among the various DIV on each device for any of the chemical challenges (ESI Fig. 1†). Additionally, responses to each chemical stimulus were similar when comparing the devices; no significance was observed ($p > 0.05$).

The chemically evoked responses obtained from the hDRG neurons on our MEA platform were in agreement with reports in the literature for these chemical stimuli on spike duration and frequency.[62,63] As expected, spike train duration after exposure to capsaicin was generally longer compared to the duration of responses for ATP, which typically produces a quick burst of activity for a short duration (<30 seconds).[64,65] Additionally, hDRG neurons responded to KCl with fewer action potentials (compared to ATP or capsaicin), followed by a cease in activity.

The interspike interval (ISI), the time between individual action potentials within a spike train, and the total number of spikes collected within 90 seconds of recording are shown in Fig. 7. Individual ISI distributions for hDRG neurons over DIV in response to ATP (Fig. 7A), capsaicin (Fig. 7B) and KCl (Fig. 7C) illustrate the variations in response observed for the
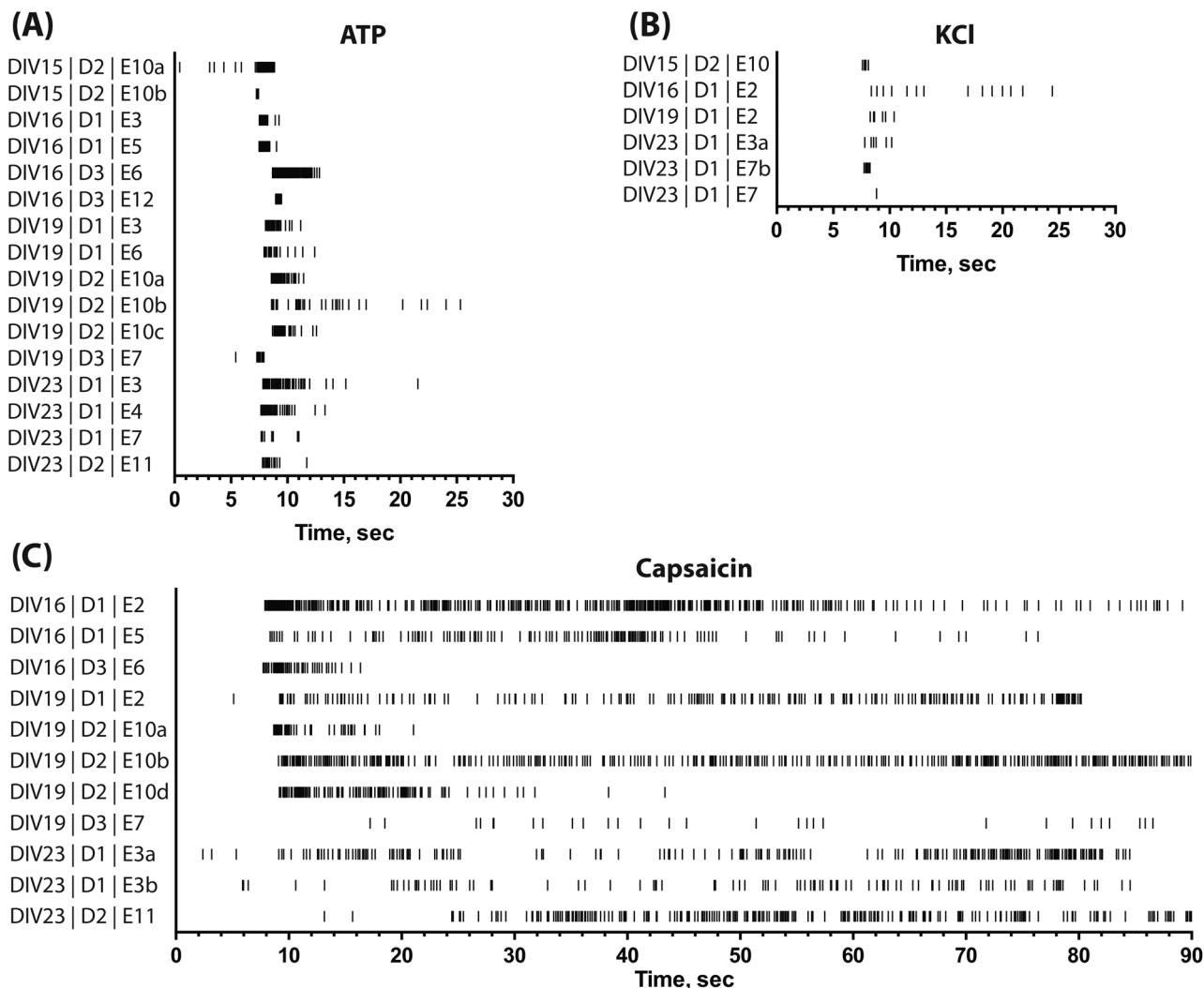
Fig. 6 Raster plot visualization of hDRG responses to each chemical challenge. Each black line represents the occurrence of a spike. Evoked responses upon stimulation with ATP (A), KCl (B) and capsaicin (C) are shown for individual electrodes through DIV23. Raster data identifiers are composed of DIV, device number (D) and electrode number (E). If signals from multiple neurons are discerned for a single electrode, neuron identifiers are used (*e.g.* a, b, c).

individual neurons upon stimulation. The median ISI values for individual neurons exposed to each chemical are represented in Fig. 7D. For ATP, the average median ISI was 0.067 ± .048 s, which was shorter than those for capsaicin (0.348 ± 0.428 s) and KCl (0.366 ± .314 s). Differences in the average median ISI among groups were present (1-way ANOVA, $p < 0.05$), but only the pairwise comparison between ATP *vs.* CAP was statistically significant (Tukey's multiple comparison test). In terms of overall spikes, capsaicin-evoked responses resulted in a greater number of total spikes (153.8 ± 110.2) (Fig. 7E) than ATP (30.3 ± 18.7) and KCl (7.6 ± 3.6). Again, the total number of spikes varied between stimuli (1-way ANOVA, $p < 0.05$), and all but ATP *vs.* KCl were statistically significant (Tukey's multiple comparison test) (Fig. 7).

Finally, using the logarithms of the median ISI and spike number as features, cluster analysis revealed characteristic sig-

natures for each chemical stimulus (Fig. 7F). This approach to "fingerprinting" evoked extracellular responses with a MEA upon chemical stimulation can be used to identify alterations in response for human DRG neurons after acute or chronic toxicant or drug exposure.

Conclusion

In this study, we have developed and validated a MEA platform that is suitable for repeated long-term assessment of the neuronal health and function of hDRG neuronal cultures. This platform enabled the simultaneous measurement of both optical and electrophysiological responses upon chemical stimulation. We successfully recorded responses from chemical stimuli, such as ATP and capsaicin, repeatedly through
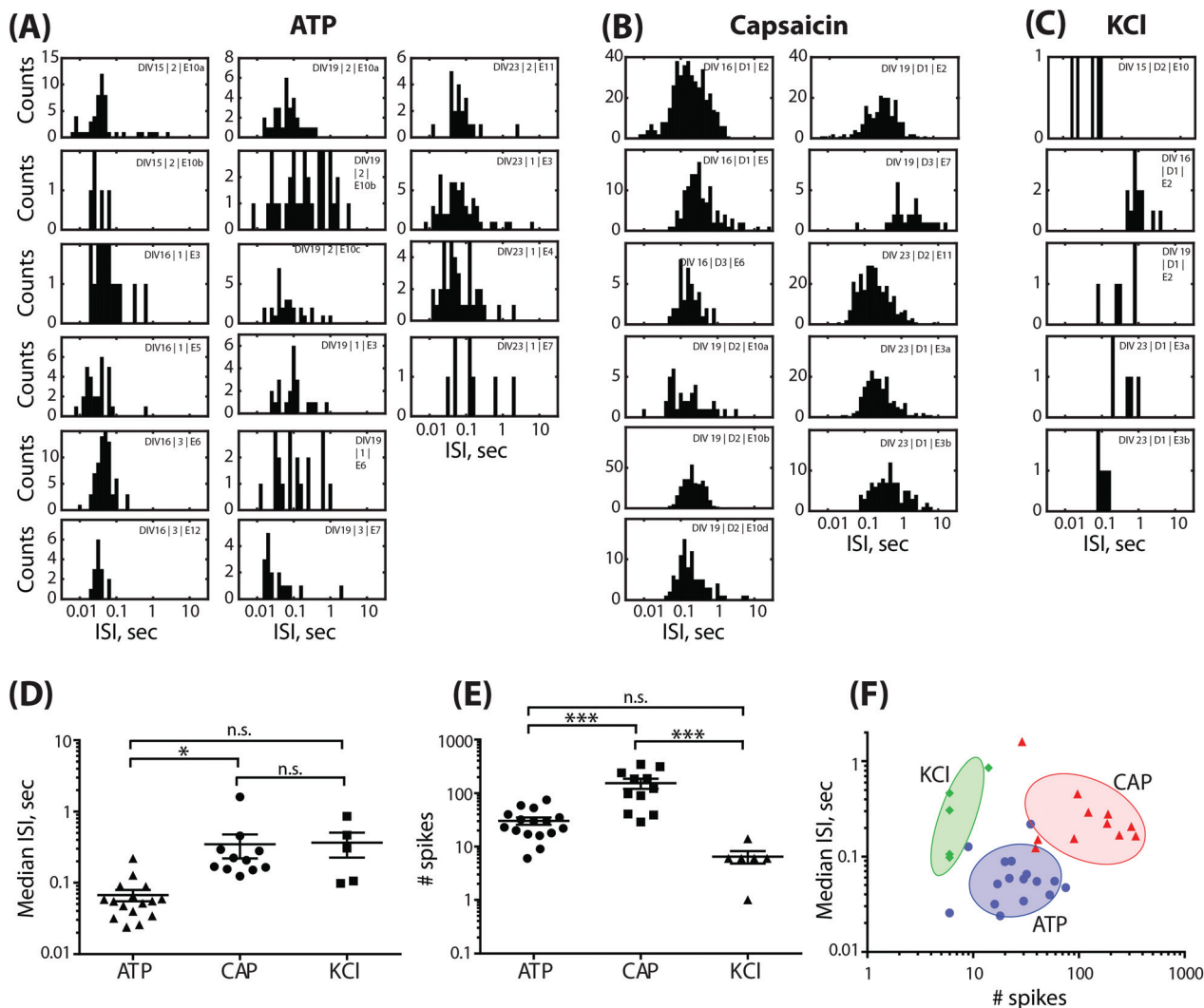
Fig. 7 Features of electrophysiological recordings for each chemical exposure. (A–C) Histograms of interspike intervals (ISI) for each chemical stimulant. (A) ATP, (B) capsaicin (CAP), (C) KCl. (D) Median ISI values and (E) the number of spikes for individual neurons in response to each chemical stimulant. Spike number reflects a 90 second time period following stimulant injection. The means and error bars representing SEM are shown. Pairwise statistical significance determined using a Tukey's multiple comparison test (*$p < 0.05$; ***$p < 0.001$; n.s. = no significance). (F) Correlation of ISI and spike number for individual neurons demonstrates the clustered response to a chemical stimulant (ATP = circle; CAP = triangle; KCl = diamond). Shaded areas are confidence ellipses corresponding to 1 S.D.

DIV23. Importantly, this is the first MEA platform to incorporate and evaluate the long-term function and health of human DRG neuronal cultures.

Optical and electrophysiological recordings identified distinct hDRG activity in response to the chemical challenges presented, demonstrating the potential to non-invasively classify physiologically meaningful responses to different stimuli. This MEA platform provides a unique opportunity to simultaneously record a variety of nociceptive responses as well as the activity of the voltage-gated channels responsible for transmitting the peripheral responses to the CNS. These non-invasive measures will provide informative short- and long-term data when investigating the neurotoxic potential of toxicants and drugs in the peripheral nervous system. The MEA that was incorporated into the platform for this study had a relatively

small number of electrodes within a simple grid geometry. This simplicity was favorable for building and validating the prototype chip-based human tissue platform. Higher numbers of electrodes with customized arrangements and coatings are being developed for future generations of devices, with the aim of developing *in vitro* platforms with multiple tissue types and multi-modal sensing. Ultimately, this platform will offer a valuable drug or toxicant screening tool that provides physiologically relevant data about the neuron function.

Author contributions

H. A. E. designed and performed experiments, data analysis and contributed to manuscript preparation. S. H. F. performed

experiments, electrophysiology data analysis and contributed to manuscript preparation. N. O. F. performed experiments, data analysis and statistics and contributed to manuscript preparation. E. M. carried out device fabrication. D. S. assisted in device fabrication and manuscript preparation. M. M. contributed to the experimental design. J. Z., G. P., P. M. and A. G. acquired human donor tissue, cultured human neuronal cultures and contributed to the manuscript. E. K. W., K. K. and S. P. contributed to the experimental design and manuscript preparation.

Acknowledgements

References

1 N. Shanks, R. Greek and J. Greek, Are animal models predictive for humans?, *Philos. Ethics Humanit. Med.*, 2009, **4**(1), 2.

2 I. W. Y. Mak, N. Evaniew and M. Ghert, Lost in translation: animal models and clinical trials in cancer treatment, *Am. J. Transl. Res.*, 2014, **6**(2), 114–118.

3 M. B. Esch, T. L. King and M. L. Shuler, The role of body-on-a-chip devices in drug and toxicity studies, *Annu. Rev. Biomed. Eng.*, 2011, **13**(1), 55–72.

4 T. Kaneko, *et al.*, On-chip in vitro cell-network pre-clinical cardiac toxicity using spatiotemporal human cardiomyocyte measurement on a chip, *Sci. Rep.*, 2014, **4**, 4670.

5 A. E. Dubin and A. Patapoutian, Nociceptors: the sensors of the pain pathway, *J. Clin. Invest.*, 2010, **120**(11), 3760–3772.

6 G. T. Young, *et al.*, Characterizing human stem cell-derived sensory neurons at the single-cell level reveals their ion channel expression and utility in pain research, *Mol. Ther.*, 2014, **22**(8), 1530–1543.

7 K. J. Bar, *et al.*, GDNF and its receptor component Ret in injured human nerves and dorsal root ganglia, *NeuroReport*, 1998, **9**(1), 43–47.

8 P. Facer, *et al.*, Differential expression of the capsaicin receptor TRPV1 and related novel receptors TRPV3, TRPV4 and TRPM8 in normal human tissues and changes in traumatic and diabetic neuropathy, *BMC Neurol.*, 2007, **7**, 11.

9 J. Patil, *et al.*, Intraneuronal angiotensinergic system in rat and human dorsal root ganglia, *Regul. Pept.*, 2010, **162**(1–3), 90–98.

10 G. D. Smith, *et al.*, TRPV3 is a temperature-sensitive vanilloid receptor-like protein, *Nature*, 2002, **418**(6894), 186–190.

11 K. Coward, *et al.*, Sodium channel beta 1 and beta 2 subunits parallel SNS/PN3 alpha-subunit changes in injured human sensory neurons, *NeuroReport*, 2001, **12**(3), 483–488.

12 K. Coward, *et al.*, Immunolocalization of SNS/PN3 and NaN/SNS2 sodium channels in human pain states, *Pain*, 2000, **85**(1–2), 41–50.

13 U. Anand, *et al.*, Angiotensin II type 2 receptor (AT(2)R) localization and antagonist-mediated inhibition of capsaicin responses and neurite outgrowth in human and rat sensory neurons, *Eur. J. Pain*, 2013, **17**(7), 1012–1026.

14 U. Anand, *et al.*, Cytosine arabinoside affects the heat and capsaicin receptor TRPV1 localisation and sensitivity in human sensory neurons, *J. Neuro-Oncol.*, 2008, **89**(1), 1–7.

15 U. Anand, *et al.*, The effect of neurotrophic factors on morphology, TRPV1 expression and capsaicin responses of cultured human DRG sensory neurons, *Neurosci. Lett.*, 2006, **399**(1–2), 51–56.

16 U. Anand, *et al.*, TRPA1 receptor localisation in the human peripheral nervous system and functional studies in cultured human and rat sensory neurons, *Neurosci. Lett.*, 2008, **438**(2), 221–227.

17 U. Anand, *et al.*, Cannabinoid receptor CB2 localisation and agonist-mediated inhibition of capsaicin responses in human sensory neurons, *Pain*, 2008, **138**(3), 667–680.

18 A. Y. Valeyev, *et al.*, Pentobarbital-activated Cl- channels in cultured adult and embryonic human DRG neurons, *Dev. Brain Res.*, 2000, **124**(1–2), 137–140.

19 A. Y. Valeyev, *et al.*, Alphaxalone activates a Cl-conductance independent of GABA(A) receptors in cultured embryonic human dorsal root ganglion neurons, *J. Neurophysiol.*, 1999, **82**(1), 10–15.

20 A. Y. Valeyev, *et al.*, GABA-induced Cl- current in cultured embryonic human dorsal root ganglion neurons, *J. Neurophysiol.*, 1999, **82**(1), 1–9.

21 A. Y. Valeyev, *et al.*, Pharmacologically novel GABA receptor in human dorsal root ganglion neurons, *J. Neurophysiol.*, 1996, **76**(5), 3555–3558.

22 F. N. Maddox, *et al.*, GABA(A) receptor subunit mRNA expression in cultured embryonic and adult human dorsal root ganglion neurons, *Dev. Brain Res.*, 2004, **149**(2), 143–151.

23 T. K. Baumann, *et al.*, Responses of adult human dorsal root ganglion neurons in culture to capsaicin and low pH, *Pain*, 1996, **65**(1), 31–38.

24 S. D. Dib-Hajj, *et al.*, Two tetrodotoxin-resistant sodium channels in human dorsal root ganglion neurons, *FEBS Lett.*, 1999, **462**(1–2), 117–120.

25 S. Acharjee, *et al.*, HIV-1 viral protein R causes peripheral nervous system injury associated with in vivo neuropathic pain, *FASEB J.*, 2010, **24**(11), 4343–4353.

26 S. Davidson, *et al.*, Human sensory neurons: membrane properties and sensitization by inflammatory mediators, *Pain*, 2014, **155**(9), 1861–1870.

27 U. Anand, *et al.*, Cytosine arabinoside affects the heat and capsaicin receptor TRPV1 localisation and sensitivity in human sensory neurons, *J. Neuro-Oncol.*, 2008, **89**(1), 1–7.

28 P. Facer, *et al.*, Differential expression of the capsaicin receptor TRPV1 and related novel receptors TRPV3, TRPV4 and TRPM8 in normal human tissues and changes in traumatic and diabetic neuropathy, *BMC Neurol.*, 2007, **7**, 11–11.

29 F. N. Maddox, *et al.*, GABAA receptor subunit mRNA expression in cultured embryonic and adult human dorsal root ganglion neurons, *Brain Res. Dev. Brain Res.*, 2004, **149**(2), 143–151.

30 S. M. Potter and T. B. DeMarse, A new approach to neural cell culture for long-term studies, *J. Neurosci. Methods*, 2001, **110**(1–2), 17–24.

31 L. J. Breckenridge, *et al.*, Advantages of using microfabricated extracellular electrodes for in vitro neuronal recording, *J. Neurosci. Res.*, 1995, **42**(2), 266–276.

32 T. J. Heikkila, *et al.*, Human embryonic stem cell-derived neuronal cells form spontaneously active neuronal networks in vitro, *Exp. Neurol.*, 2009, **218**(1), 109–116.

33 T. Tanaka, *et al.*, In vitro pharmacologic testing using human induced pluripotent stem cell-derived cardiomyocytes, *Biochem. Biophys. Res. Commun.*, 2009, **385**(4), 497–502.

34 A. F. Johnstone, *et al.*, Microelectrode arrays: a physiologically based neurotoxicity testing platform for the 21st century, *Neurotoxicology*, 2010, **31**(4), 331–350.

35 M. Frega, *et al.*, Cortical cultures coupled to micro-electrode arrays: a novel approach to perform in vitro excitotoxicity testing, *Neurotoxicol. Teratol.*, 2012, **34**(1), 116–127.

36 M. A. Nassar, *et al.*, Nociceptor-specific gene deletion reveals a major role for Nav1.7 (PN1) in acute and inflammatory pain, *Proc. Natl. Acad. Sci. U. S. A.*, 2004, **101**(34), 12706–12711.

37 J. J. Cox, *et al.*, An SCN9A channelopathy causes congenital inability to experience pain, *Nature*, 2006, **444**(7121), 894–898.

38 K. H. Kim and S. J. Kim, Neural spike sorting under nearly 0-dB signal-to-noise ratio using nonlinear energy operator and artificial neural-network classifier, *IEEE Trans. Biomed. Eng.*, 2000, **47**(10), 1406–1411.

39 S. Kim and J. McNames, Automatic spike detection based on adaptive template matching for extracellular neural recordings, *J. Neurosci. Methods*, 2007, **165**(2), 165–174.

40 R. Chandra and L. M. Optican, Detection, classification, and superposition resolution of action potentials in multi-unit single-channel recordings by an on-line real-time neural network, *IEEE Trans. Biomed. Eng.*, 1997, **44**(5), 403–412.

41 M. S. Lewicki, Bayesian Modeling and Classification of Neural Signals, *Neural Comput.*, 1994, **6**(5), 1005–1030.

42 N. V. Swindale and M. A. Spacek, Spike detection methods for polytrodes and high density microelectrode arrays, *J. Comput. Neurosci.*, 2015, **38**(2), 249–261.

43 K. G. Oweiss and D. J. Anderson, A unified framework for advancing array signal processing technology of multi-channel microprobe neural recording devices, in *2nd Annual International IEEE-EMB Special Topic Conference on Microtechnologies in Medicine & Biology*, 2002.

44 S. Mukhopadhyay and G. C. Ray, A new interpretation of nonlinear energy operator and its efficacy in spike detection, *IEEE Trans. Biomed. Eng.*, 1998, **45**(2), 180–187.

45 R. K. Mehra and J. Peschon, An innovations approach to fault detection and diagnosis in dynamic systems, *Automatica*, 1971, **7**(5), 637–640.

46 A. S. Willsky and H. L. Jones, A generalized likelihood ratio approach to the detection and estimation of jumps in linear systems, *IEEE Trans. Autom. Control*, 1976, **21**(1), 108–112.

47 V. Kadirkamanathan, *et al.*, Particle filtering-based fault detection in non-linear stochastic systems, *Int. J. Syst. Sci.*, 2002, **33**(4), 259–265.

48 J. V. Candy, *et al.*, Model-based failure detection for cylindrical shells from noisy vibration measurements, *J. Acoust. Soc. Am.*, 2014, **136**(6), 3114.

49 M. S. Lewicki, A review of methods for spike sorting: the detection and classification of neural action potentials, *Network: Comput. Neural Syst.*, 1998, **9**(4), 53–78.

50 F. O. Morin, Y. Takamura and E. Tamiya, Investigating neuronal activity with planar microelectrode arrays: achievements and new perspectives, *J. Biosci. Bioeng.*, 2005, **100**(2), 131–143.

51 S. Martinoia, *et al.*, A general-purpose system for long-term recording from a microelectrode array coupled to excitable cells, *J. Neurosci. Methods*, 1993, **48**(1), 115–121.

52 O. Kaiser, *et al.*, Dissociated neurons and glial cells derived from rat inferior colliculi after digestion with papain, *PLoS One*, 2013, **8**(12), e80490.

53 P. H. O'Lague, *et al.*, Evidence for cholinergic synapses between dissociated rat sympathetic neurons in cell culture, *Proc. Natl. Acad. Sci. U. S. A.*, 1974, **71**(9), 3602–3606.

54 U. Egert, D. Heck and A. Aertsen, Two-dimensional monitoring of spiking networks in acute brain slices, *Exp. Brain Res.*, 2002, **142**(2), 268–274.

55 D. A. Henze, *et al.*, Intracellular features predicted by extracellular recordings in the hippocampus in vivo, *J. Neurophysiol.*, 2000, **84**(1), 390–400.

56 A. Odawara, *et al.*, Long-term electrophysiological activity and pharmacological response of a human induced pluripotent stem cell-derived neuron and astrocyte co-culture, *Biochem. Biophys. Res. Commun.*, 2014, **443**(4), 1176–1181.

57 L. Ylä-Outinen, *et al.*, Human cell-based micro electrode array platform for studying neurotoxicity, *Front. Neuroeng.*, 2010, **3**, 111.

58 E. Biffi, *et al.*, The influence of neuronal density and maturation on network activity of hippocampal cell cultures: a methodological study, *PLoS One*, 2013, **8**(12), e83899.

59 M. S. Schroeter, *et al.*, Emergence of rich-club topology and coordinated dynamics in development of hippocampal functional networks in vitro, *J. Neurosci.*, 2015, **35**(14), 5459–5470.

60 M. E. J. Obien, *et al.*, Revealing neuronal function through microelectrode array recordings, *Front. Neurosci.*, 2015, 8.

61 D. Wagenaar, T. B. DeMarse and S. M. Potter, MeaBench: A toolset for multi-electrode data acquisition and on-line analysis, in *2nd International IEEE EMBS Conference on Neural Engineering, 2005, Conference Proceedings*, 2005.

62 M. Kollarik, *et al.*, Capsaicin-sensitive and -insensitive vagal bronchopulmonary C-fibres in the mouse, *J. Physiol.*, 2003, **551**(Pt 3), 869–879.

63 Y. V. Medvedeva, M. S. Kim and Y. M. Usachev, Mechanisms of prolonged presynaptic Ca^{2+} signaling and glutamate release induced by TRPV1 activation in rat sensory neurons, *J. Neurosci.*, 2008, **28**(20), 5295–5311.

64 P. M. Dunn, Y. Zhong and G. Burnstock, P2X receptors in peripheral neurons, *Prog. Neurobiol.*, 2001, **65**(2), 107–134.

65 J. G. Gu and A. B. MacDermott, Activation of ATP P2X receptors elicits glutamate release from sensory neuron synapses, *Nature*, 1997, **389**(6652), 749–753.